Tuning the Size, Shape and Density of γ'-Ga$_y$Fe$_{4-y}$N Nanocrystals Embedded in GaN

Andrea Navarro-Quezada *[ID], Thibaut Devillers †[ID], Tian Li and Alberta Bonanni

Institute for Semiconductor and Solid-State Physics, Johannes Kepler University Linz, Altenberger Str. 69, 4040 Linz, Austria; thibaut.devillers@neel.cnrs.fr (T.D.); litianun@126.com (T.L.); alberta.bonanni@jku.at (A.B.)

* Correspondence: andrea.navarro-quezada@jku.at; Tel.: +43-732-2468-9622

† Current address: Institute Néel, CNRS, 25 rue des Martyrs BP 166, 38042 Grenoble, France.

Abstract: Phase-separated semiconductor systems hosting magnetic nanocrystal (NCs) are attracting increasing attention, due to their potential as spintronic elements for the next generation of devices. Owing to their morphology- and stoichiometry-dependent magnetic response, self-assembled γ'-Ga$_y$Fe$_{4-y}$N NCs embedded in a Fe δ-doped GaN matrix, are particularly versatile. It is studied and reported here, how the tuning of relevant growth parameters during the metalorganic vapour phase epitaxy process affects the crystalline arrangement, size, and shape of these self-assembled nanostructures. In particular, it is found that the Ga-flow provided during the δ-doping , determines the amount of Fe incorporated into the layers and the spatial density of the NCs. Moreover, the in-plane dimensions of the NCs can also be controlled via the Ga-flow, conditioning the aspect-ratio of the embedded nanostructures. These findings are pivotal for the design of nanocrystal arrays with on-demand size and shape, essential requirements for the implementation into functional devices.

Keywords: magnetic nanocrystals, Metal-organic vapor phase epitaxy, III-nitrides

1. Introduction

The range of functionalities of technologically relevant semiconductors like e.g., Si, GaAs, and GaN can be significantly widened by adding transition metal (TM) ions during the epitaxial growth processes employed for the fabrication of semiconductor heterostructures. In this context, a fundamental *caveat* is represented by the actual incorporation of the TM ions into the semiconducting matrix, since this affects dramatically the structural, chemical, optical and magnetic properties of the resulting structure. In particular, depending on the growth conditions, the magnetic species are incorporated either homogeneously, substituting original lattice cations and producing a dilute magnetic semiconductor (DMS) [1] or anisotropically, inducing either crystallographic or chemical phase separation and spinodal nanodecomposition and driving the system to the state of a condensed magnetic semiconductor (CMS) [2,3].

The incorporation of TM ions into III-nitride epitaxial systems has recently opened wide perspectives for spin-dependent functionalities in these material systems. In particular, in the DMS (Ga,Mn)N, the significant inversion asymmetry of the wurtzite structure allows magnetization manipulation by means of an electric field through the inverse piezoelectric effect [4]. On the other hand, in (Ga,Fe)N fabricated by metal-organic vapor phase epitaxy (MOVPE), the incorporation of Fe ions above the solubility limit drives the system to a CMS state, with the self-assembly of planar arrays of magnetic Fe$_x$N nanocrystals (NCs) ($x = 1, 2, 3, 4$) embedded in the GaN matrix [5–8], expected to provide an efficient, robust and energy-saving platform in particular for magnetic data storage [9–12] and for the generation of polarized spin currents [13,14].

It has been previously shown that the fabrication conditions during the MOVPE of GaN layers doped with Fe above the solubility limit play a crucial role in the chemical and structural characteristics of the embedded NCs. In particular, the growth temperature was found to affect the crystalline structure as well as the chemical composition of the NCs, allowing for selecting the magnetic response to be ferromagnetic (FM)—for γ'-Fe$_4$N and ϵ-Fe$_3$N—or antiferromagnetic (AF)—for ζ-Fe$_2$N [7]. Through the homogeneous incorporation of Si donors and Mg acceptors, the formation of the Fe$_x$N NCs is hindered [15,16], while the addition of Mg cations in a δ-like fashion promotes the self-assembly of the NCs [16].

Furthermore—by employing a δ-growth mode—the control over the spatial distribution and over the formation of single crystalline phase γ'-Ga$_y$Fe$_{4-y}$N NCs embedded in GaN, showing a strong uniaxial magnetic anisotropy with three in-plane easy axes, was successfully achieved [8,17]. Moreover, the in-plane magnetic anisotropy, characteristic of these systems, was found to trigger anisotropic magnetoresistance effects related to the transport of spin-polarized currents through the NCs at temperatures below 10 K [18].

Recently, it was demonstrated that the Mn co-doping of δ-doped (Ga,Fe)N layers hosting γ'-Ga$_y$Fe$_{4-y}$N NCs leads to a reduction in the size and sheet density of the nanocrystals, associated with the competition of Mn and Fe ions for the Ga cation sites, with consequent enhancement of the paramagnetic response from the matrix and reduction of the FM contribution from the NCs [19]. Due to the fact that in these material systems the overall magnetic characteristics of the layers are dictated by the magnetic properties of the NCs, it becomes imperative to control their size, shape and density, in view of reliable applications.

In this work, the role of the critical fabrication parameters that allow for imposing on-demand the size, shape and density of γ'-Ga$_y$Fe$_{4-y}$N NCs embedded in GaN and fabricated by MOVPE is analyzed. Specifically, it is shown that the Ga-flow and its inter-play with Fe determine the NC density and allow controlling the NC size and shape.

2. Materials and Methods

The layers presented in this work are grown by MOVPE in an Aixtron 200X horizontal reactor system (Aixtron, Achen, Germany) on *c*-plane [0001] sapphire (Al$_2$O$_3$) substrates using trimethylgallium (TMGa), ammonia (NH$_3$) and ferrocene (Cp$_2$Fe) as precursors. Upon deposition of a low-temperature GaN nucleation layer (NL) at 540 °C, followed by annealing in NH$_3$ at 1040 °C, a 1000 nm high-quality GaN buffer layer is deposited at 1040 °C with a TMGa flow of 25 standard cubic centimeters per minute (sccm) and 1500 sccm of NH$_3$, followed by a Fe-doped GaN (GaδFeN) layer at 780 °C using a δ-like growth mode, i.e., by alternately opening and closing the TMGa source, while keeping the Cp$_2$Fe and NH$_3$ sources open (GaN:Fe/Fe:N). All the bubblers are kept at 1 atm pressure, while the temperature is 0 °C for TMGa and 17 °C for the Cp$_2$Fe source. Each δ-growth period has a total duration of 1 min and consists of 10 s of GaN:Fe and 50 s of FeN. The GaδFeN layers are covered by a GaN capping layer, whose thickness determines the position of the array of γ'-Ga$_y$Fe$_{4-y}$N nanocrystals stabilized through the δ-procedure below the sample surface [8]. The distribution of the NCs in the GaN matrix along the growth *c*-direction, as well as the NC sheet density, size and shape, has been investigated by transmission electron microscopy (TEM) measurements. The crystallographic phase of the NCs is established from high-resolution TEM (HRTEM) images and selective-area diffraction pattern analysis. The TEM specimens are prepared by mechanical polishing, dimpling and ion milling in a Gatan Precision Ion Polishing System (Gatan, Munich, Germany). Dark-field and bright-field measurements in conventional mode have been performed using a JEM 2000 EX JEOL microscope (Jeol, Tokyo, Japan). A schematic representation of the samples architecture is shown in Figure 1a, while in Figure 1b a cross-section TEM image evidences the relevant regions in the samples.
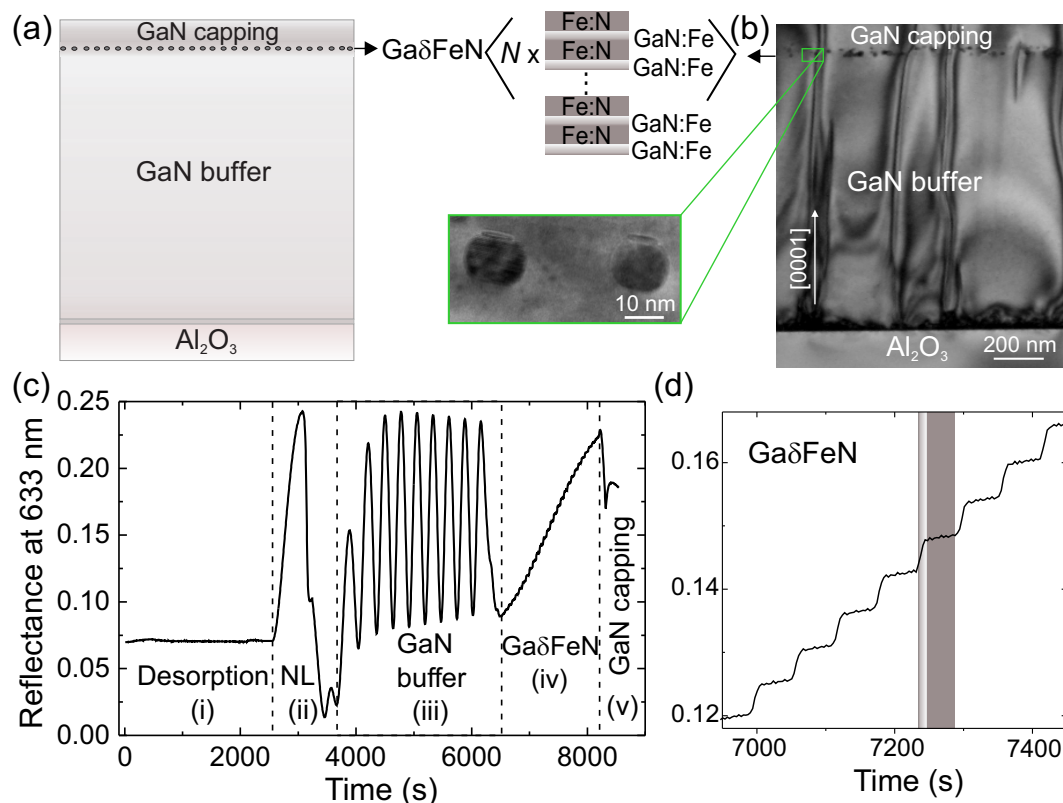
Figure 1. (**a**) Schematic representation of the samples architecture; (**b**) Transmission electron microscopy (TEM) cross-section micrograph showing the relevant regions in a representative sample and the presence of the planar array of NCs; (**c**) In situ reflectance acquired at 633 nm during deposition indicating the MOVPE fabrication steps described in the text and labeled (i) to (vi); (**d**) Close-up of the in situ reflectance acquired during the growth of GaδFeN. The light grey and dark grey vertical lines indicate the growth of the GaN:Fe and Fe:N steps, respectively.

During the fabrication of the GaδFeN layers, the following parameters are principally controlled: the TMGa source flow, the NH_3 source flow, the Cp_2Fe source flow, the number N of GaN:Fe/Fe:N δ-grown periods (Figure 1a,b), the time employed to grow a period, and the deposition time of each individual step in a period. For this work, series of samples are considered, in which the Ga-flow or the number of periods are varied along the sample series. Details on the samples and on their fabrication parameters are summarized in Table 1. The total Ga-flow (normalized Ga-flow) provided during fabrication is calculated by multiplying the TMGa source flow in sccm by: the time t_{Ga} during which the TMGa source is kept open during the δ-period, and by the number N of periods.

Table 1. Relevant fabrication parameters employed for the fabrication of the phase-separated samples.

Sample	TMGa (sccm)	Cp_2Fe (sccm)	NH_3 (sccm)	N	t_{Ga} (s)	T_{GaFeN} ± 5 (nm)	Normalized Ga-Flow
S1544	5.0	450	800	30	10	66	24.9
S1547	5.0	450	800	15	10	46	12.5
S1559	2.5	450	800	15	10	40	6.2
S1656	2.0	450	800	15	10	33	4.9

The entire growth process is monitored in situ and online by optical reflectance using a LayTec EpiTT-L reflectometer (LayTec, Berlin, Germany) that allows following the evolution of the reflectance at three different wavelengths: 950 nm, 633 nm and 405 nm, respectively. In Figure 1c, an exemplary reflectance spectrum acquired at 633 nm during the growth process is depicted, and the single

fabrication steps are identified as: (i) substrate desorption in H_2 at 1100 °C, (ii) nucleation layer (NL) growth at 540 °C followed by annealing under NH_3 at 1040 °C, (iii) GaN buffer layer deposition, (iv) growth of the GaδFeN at 780 °C, and (v) deposition of the GaN capping layer at 950 °C. The thickness of the different layers is obtained by fitting the oscillations in the reflectance spectrum according to the procedures described in Ref. [20].

Each period GaN:Fe/Fe:N of the GaδFeN sequence is reflected in a step in the kinetic reflectance measurement, specifically: during the GaN:Fe deposition, the reflectance signal increases—confirming the growth of GaN:Fe—and during the Fe:N deposition it remains constant, as shown in Figure 1d. The stability of the reflectance signal during the time in which the TMGa source is closed is attributed to the onset of an etching mechanism, which competes with the growth and eventually hinders it [20].

High-resolution X-ray diffraction (HRXRD) rocking-curves acquired along the [0001] growth direction are employed to analyze the sample structure and the nanocrystals' crystallographic phase. The measurements are carried out in a PANalytical X'Pert Pro Material Research Diffractometer (Malvern Panalytical, Nürnberg, Germany) with a hybrid monochromator equipped with a 0.25 ° divergence slit and a PixCel detector using 19 channels for detection and a 5 mm anti-scatter slit. The average size of the nanocrystals along the growth direction (h) is obtained from the full-width at half-maximum (FWHM) of the NC diffraction peak employing the Scherrer formula [21]. The magnetic properties of the GaδFeN thin layers have been measured in a Quantum Design superconducting quantum interference device (SQUID) MPMS XL magnetometer at room-temperature according to the procedure described elsewhere [22,23].

3. Results

3.1. Crystal Structure

The HRXRD rocking-curves collected along the [0001] growth direction are reported in Figure 2a for all relevant samples. The (0002) and (0004) diffraction peaks for GaN, the (0006) from the Al_2O_3 substrate and the (200) from the embedded face-centered cubic (fcc) γ'-$Ga_yFe_{4-y}N$ nanocrystals are detected, confirming the previously reported epitaxial relation between the NCs and the GaN matrix along the growth direction, namely: $[001]_{NC} \parallel [0001]_{GaN}$ [8]. The full epitaxial relation was already identified by us as $[001]_{NC} \parallel [0001]_{GaN}$ and $(001)[110]_{NC} \parallel (0001)[11\bar{2}0]_{GaN}$, with 12 equivalent in-plane orientations of the NCs, with their basal plane maintaining a parallel orientation with respect to the one of GaN.

By analyzing the series of samples in which the Ga-flow is decreased—for successive samples—during the deposition of GaδFeN: a decrease in the γ'-$Ga_yFe_{4-y}N$ 200 peak intensity and a shift of the peak maximum to higher diffraction angles (with decreasing Ga-flow), are observed, pointing at a reduction of the lattice parameter a.

The lattice parameter a obtained from the HRXRD diffraction peaks is reported as a function of the Ga-flow in Figure 2b, where the decrement of a with decreasing Ga-flow is confirmed. In fact, in the samples fabricated under Ga-rich conditions, the incorporation of Ga atoms into γ'-Fe_4N is favored and reflected in the increment of the lattice parameter a. The Ga atoms which substitute the Fe atoms exclusively at the Wyckoff lattice positions, have an atomic radius of $r_{Ga} = 0.141$ nm, which is larger than the one of the Fe atoms ($r_{Fe} = 0.124$ nm) [24]. The change in lattice parameter with Ga incorporation has been previously reported for γ'-$Ga_yFe_{4-y}N$ nanoparticles prepared by two-step ammonolysis synthesis [24] and for γ'-$Ga_yFe_{4-y}N$ embedded NCs in GaN fabricated by MOVPE with varying TMGa source flows [8].

The incorporation of Ga ions into the γ'-Fe_4N structure weakens the ferromagnetic coupling between Fe ions, reduces the magnetic moment of the system, and the magnetic properties of γ'-$Ga_yFe_{4-y}N$ can be modulated between FM ($y \leq 25$) and weakly AF ($y \geq 25$) [25]. The magnetic response of the GaδFeN layers analyzed here is characterized by two main contributions, namely: (i) a paramagnetic one arising from the Fe ions that substitute for the Ga cations in the matrix, and (ii) a

superparamagnetic one generated by the embedded nanocrystals [5,7,23]. Furthermore, the magnetic field required to saturate the magnetic moment of the layers at room-temperature decreases with the Ga-flow. This is shown in the inset to Figure 2b and is consistent with the fact that the less Ga is present in the lattice, the stronger is the FM signal from the NCs, leading to a swift saturation of the overall magnetic moment.
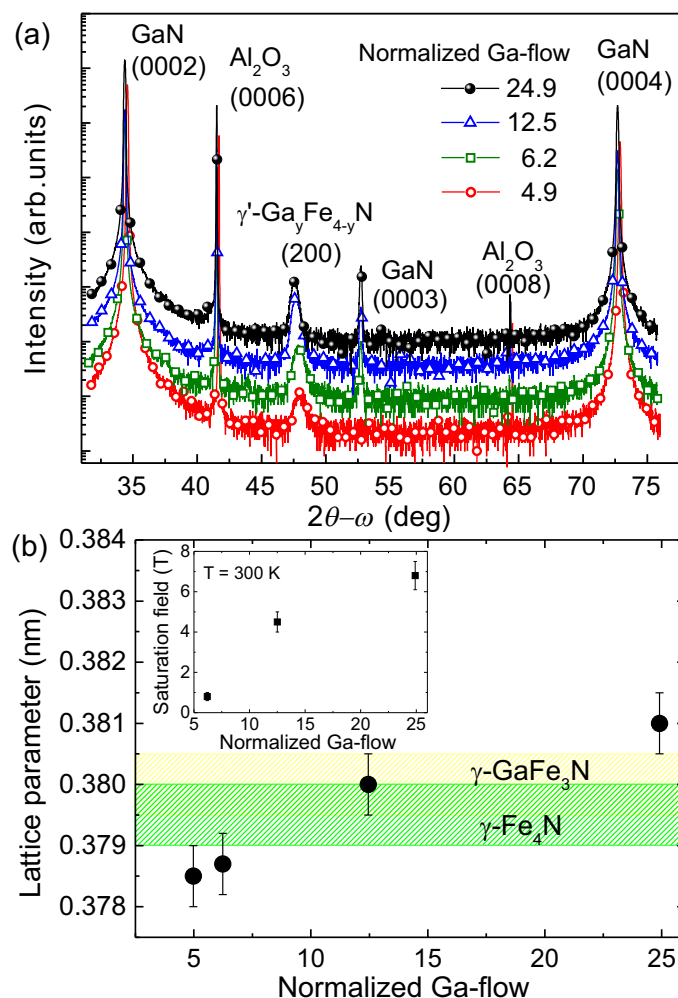

Figure 2. (**a**) High-resolution x-ray diffraction rocking-curves acquired along the [0001] direction for the series of samples fabricated employing different Ga-flows; (**b**) Lattice parameter as a function of the normalized Ga-flow showing an increment in the lattice with increasing Ga supply. Inset to (**b**): magnetic saturation field vs. normalized Ga-flow.

The observed quenching in the intensity of the (200) diffraction peak of the NCs with decreasing Ga-flow suggests either a decrease in the nanocrystal size along the growth direction or a reduction in the density of nanocrystals and the two options are discussed here below.

3.2. Size and Shape

The average h—height—of the NCs along the c-growth direction is obtained from the FWHM analysis of the diffraction peaks in the HRXRD spectra. The calculated values are listed in Table 2, together with the values obtained from a statistically significant number of HRTEM images, showing a good agreement between the two techniques. In Figure 3a, it is observed that, as h becomes shorter, less Ga-flow is provided during growth. The amount of Ga-flow during the fabrication correlates directly with the thickness of the GaδFeN layer (T_{GaFeN}), as reported in Table 1, suggesting that the layer thickness limits the size of the NCs along the growth direction. Significantly, independent of

the nominal thickness of the Gaδ layer, h is limited to a maximum of 20 nm, as observed in Figure 3a, where the average size of the NCs is reported as a function of the normalized Ga-flow. This points at a kinetic barrier that limits h, so that, once the maximum size of 20 nm is reached, the NCs further evolve only in-plane. As a consequence, the shape of the NCs can be varied from oblate-spheroids to disc-shaped by adjusting the Ga-flow provided during deposition.

Table 2. Average nanocrystal sizes h (along the c-growth direction) and w (in-plane) obtained from HRXRD and HRTEM; aspect-ratio (h/w) and the NC sheet density D_s.

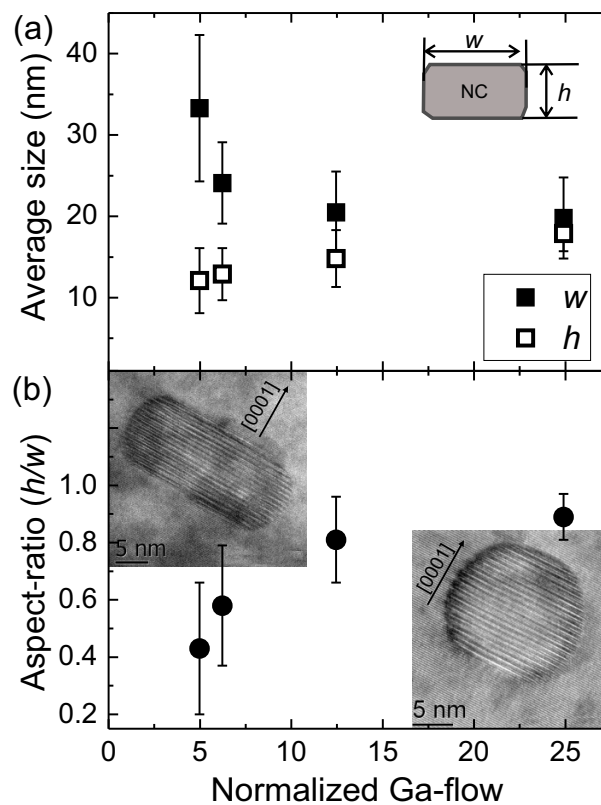| Normalized Ga-Flow	h_{HRXRD} (nm)	h_{HRTEM} (nm)	w_{HRTEM} (nm)	Aspect-Ratio (h/w)	D_s ($\pm 1.0 \times 10^9$ NC/cm^2)
24.9	16.5 ± 2.0	17.9 ± 2.2	19.8 ± 3.0	0.89 ± 0.08	15.0
12.5	14.8 ± 2.0	14.5 ± 3.2	20.5 ± 5.0	0.81 ± 0.15	2.3
6.2	12.4 ± 2.0	12.9 ± 3.5	24.1 ± 5.0	0.58 ± 0.21	3.9
4.9	10.8 ± 2.0	12.1 ± 4.0	33.4 ± 9.0	0.43 ± 0.23	7.1

Figure 3. (**a**) Nanocrystals average size: along the growth direction (h) and in-plane (w) obtained from HRXRD and HRTEM; (**b**) Aspect-ratio (h/w) as a function of the normalized Ga-flow. The cross-section HRTEM images as insets to (b) acquired along the [10$\bar{1}$0] zone axis show NCs with aspect-ratios 0.43 (left inset) and 0.95 (right inset), respectively.

In contrast, the in-plane average w—width—of the NCs, shows a broader size distribution and increases with decreasing the Ga-flow, as made evident in Figure 3a. As a consequence, the aspect-ratio of the NCs is reduced with diminishing the Ga-flow, as reported in Figure 3b. The HRTEM images presented as insets to Figure 3b confirm the change in aspect-ratio. The NC shown as left inset to Figure 3b has an aspect-ratio of 0.43 and is representative for the samples fabricated with a normalized Ga-flow of 4.9, while the one as right inset to Figure 3b has an aspect-ratio of 0.95 and is representative for the samples fabricated with a normalized Ga-flow of 24.9.

3.3. Density

The nanocrystal sheet density (D_s) for each sample is obtained from a series of plan-view HRTEM images, and is plotted as a function of the normalized Ga-flow and of the number N of GaN:Fe/Fe:N periods in Figure 4a–e. From Figure 4a, it is inferred that: (i) D_s increases with increasing Ga-flow when N is also augmented, and (ii) D_s decreases with increasing Ga-flow for samples grown with the same N ($N = 15$).

By decreasing the number of periods, the number of nanocrystals present in the layers is reduced, due to the fact that a lower absolute amount of Fe is provided to the structure. In contrast, by keeping N fixed, the density of NC increases as the Ga-flow is reduced, due to the fact that the less Ga is provided, the richer in Fe the growth conditions become.

The significant interplay of the Fe- and Ga-flow is further corroborated by comparing two samples grown respectively at a Cp_2Fe source flow of 450 sccm and 300 sccm, but both with $N = 30$. The D_s for the sample grown with 300 sccm Cp_2Fe shows a lower NC density compared to the one in the sample fabricated under a Cp_2Fe source flow of 450 sccm [8].

Based on plan-view and cross-sectional HRTEM micrographs, a rough estimation of the volume occupied by the NCs as a function of the Ga-flow has been obtained and reproduced in the lower panel of Figure 4a. In order to take into account the different aspect-ratio of the NCs, the volume is weighted by approximating a fraction (estimated from the HRTEM data) of the total number of NCs as spheres with max. radius 10 nm and the remaining ones as cylinders with a maximum axis perpendicular to the growth direction of 20 nm.

The plan-view HRTEM images in Figure 4b–e show that the NCs have a circular in-plane equilibrium shape. The size distributions obtained from the plan-view HRTEM images for the different samples are shown in the corresponding histograms in Figure 4g,h. In particular, the size distribution is narrowed with increasing N, while the average in-plane size of the NCs is reduced. The average size obtained from the histograms as a function of the normalized Ga-flow is presented in Figure 4f in accordance with the values for w obtained from the statistical analysis of a significant number of cross sectional images of NCs depicted in Figure 3a.

4. Discussion

The above results show that the following fundamental properties of γ'-$Ga_yFe_{4-y}N$ NCs embedded in GaN can be controlled by growth parameters, namely:

- **Size**: By varying N and in particular the Ga-flow, the overall thickness of the GaδFeN layer can be adjusted, allowing to tailor the NCs size. Along the c-growth direction, the size becomes smaller with decreasing Ga-flow, and does not overcome—in the range of the considered growth conditions—the maximum of 20 nm, independently of the GaδFeN layer thickness. In contrast, the in-plane diameter of the NCs increases when lowering the Ga-flow and can reach values as large as 70 nm.
- **Shape**: The modulation in the size of the NCs along either the in-plane or the growth direction affects the NC aspect-ratio, leading to changes in the NC shape from oblate-spheroids with aspect-ratios above 0.8 to disc-shaped NCs with aspect-ratios below 0.5. The higher the Ga-flow, the more homogeneous the shape distribution becomes. Previous ferromagnetic resonance (FMR) studies have shown that the shape of the nanocrystals plays a critical role in determining the values of the anisotropy tensor for each individual NC. The FMR measurements revealed a strong uniaxial out-of plane shape anisotropy attributed to the oblate-spheroid shape of the NCs [17].
- **Density**: The critical parameter for controlling D_s, is the amount of Fe provided during fabrication. The richer the Fe conditions during growth, the higher the density of NCs. This is achieved either by decreasing the Ga-flow or by increasing the number of growth periods N and the flow of the Cp_2Fe source.
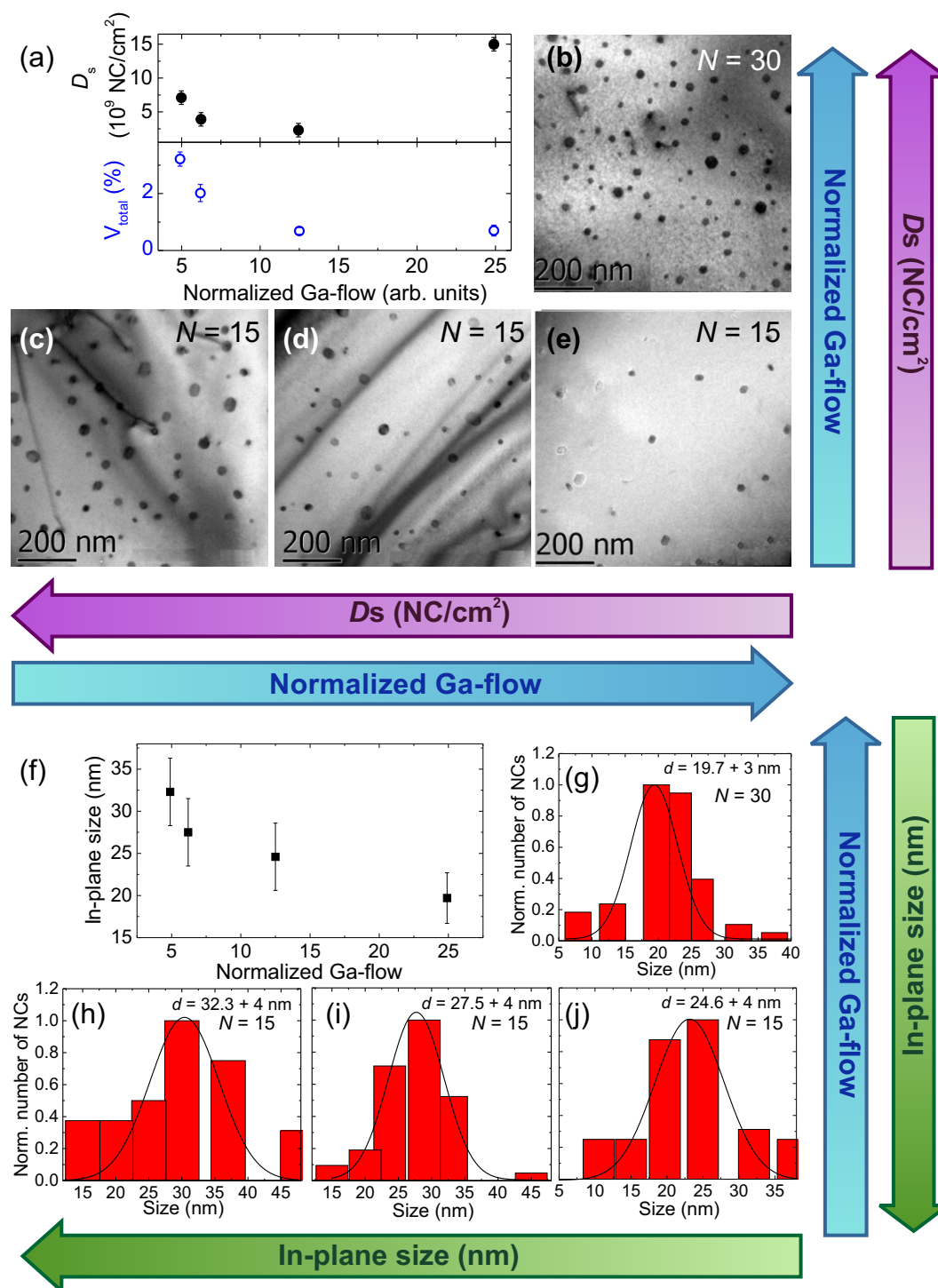
Figure 4. (**a**) Upper panel: nanocrystals' sheet density D_s as a function of the growth period N and of the Ga-flow. (**a**) Lower panel: total volume of the NCs as a function of the normalized Ga-flow (blue). HRTEM plan-view images from samples fabricated with $N = 30$ (**b**), and $N = 15$ and with decreasing Ga-flow (**c**–**e**); (**f**) Average in-plane size obtained from the size distribution histograms shown in (**g**–**j**) for the NCs obtained from the HRTEM plan-view images reported in (**b**–**e**), respectively.

An overview of the MOVPE fabrication parameters for the GaδFeN layers and their influence on the properties of embedded γ'-Ga$_y$Fe$_{4-y}$N NCs in GaN is provided in Table 3.

Table 3. Overview of the relevant MOVPE fabrication parameters and their influence on the γ'-Ga$_y$Fe$_{4-y}$N NCs embedded in GaN.

Fabrication Parameter	Adjusts
Growth period	Layer thickness, NCs sheet density, size and aspect-ratio
TMGa source flow	Layer thickness, NCs structure, size, aspect-ratio, lattice parameter, Ga incorporation into the NC [8]
Cp$_2$Fe source flow	NCs sheet density

5. Conclusions

The size, shape and density of γ'-Ga$_y$Fe$_{4-y}$N NCs embedded in a GaN matrix can be tailored by varying the fabrication conditions during an MOVPE process. Specifically, the sheet density can be adjusted on demand by either varying the number N of GaN:Fe/Fe:N periods in the δ-doping sequence, or by regulating the amount of Fe provided during growth. The size of the NCs along the c-growth direction is found to be nearly independent of the fabrication parameters, and to reach a maximum size of 20 nm. However, a reduction of N and of the Ga-flow enlarges the in-plane average size of the NCs, allowing for regulating the aspect-ratio of the NCs. This is expected to significantly affect the magnetic shape anisotropy previously observed in these GaδFeN layers [17].

For applications, it is desirable to fabricate NCs with narrow size and shape distributions. At the same time, for the study of the properties—optical, magnetic, transport—of the individual NCs, a low sheet density is highly beneficial, in order to avoid interference and interaction between the single nano-objects. It is worth noticing that increasing the number of GaN:Fe/Fe:N periods promotes the incorporation of Ga into the NCs, weakening their FM response.

The size and shape of the nanocrystals play a decisive role in the individual and overall magnetic properties of the layers. It is expected that the in-plane anisotropy, required for data-storage applications, is enhanced for the elongated disc-shaped NCs. Therefore, prospective studies of the magnetic moments of the single NCs by employing X-ray photoelectron-emission spectroscopy combined with X-ray circular dichroism [26] as a function of the size, shape and density adjusted according to the findings here reported are likely to represent the next step towards the full control and on-demand tunability of planar arrays of γ'-Ga$_y$Fe$_{4-y}$N NCs embedded in GaN.

References

1. Dietl, T. A ten-year perspective on dilute magnetic semiconductors and oxides. *Nat. Mater.* **2010**, *9*, 965–974. [CrossRef] [PubMed]
2. Dietl, T.; Sato, K.; Fukushima, T.; Bonanni, A.; Jamet, M.; Barski, A.; Kuroda, S.; Tanaka, M.; Hai, P.N.; Katayama-Yoshida, H. Spinodal nanodecomposition in semiconductors doped with transition metals. *Rev. Mod. Phys.* **2015**, *87*, 1311–1377. [CrossRef]
3. Bonanni, A.; Dietl, T. A story of high-temperature ferromagnetism in semiconductors. *Chem. Soc. Rev.* **2010**, *39*, 528–539. [CrossRef]

4. Sztenkiel, D.; Foltyn, M.; Mazur, G.; Adhikari, R.; Kosiel, K.; Gas, K.; Zgirski, M.; Kruszka, R.; Jakieła, R.; Li, T.; et al. Stretching magnetism with an electric field in a nitride semiconductor. *Nat. Commun.* **2016**, *7*, 13232. [CrossRef]

5. Bonanni, A.; Kiecana, M.; Simbrunner, C.; Li, T.; Sawicki, M.; Wegscheider, M.; Quast, M.; Przybylinska, H.; Navarro-Quezada, A.; Jakieła, R.; et al. Paramagnetic GaN:Fe and ferromagnetic (Ga,Fe)N: The relation between structural, electronic and magnetic properties. *Phys. Rev. B* **2007**, *75*, 125210. [CrossRef]

6. Li, T.; Simbrunner, C.; Navarro-Quezada, A.; Wegscheider, M.; Quast, M.; Litvinov, D.; Gerthsen, D.; Bonanni, A. Phase-dependent distribution of Fe-rich nanocrystals in MOVPE-grown (Ga,Fe)N. *J. Cryst. Growth* **2008**, *310*, 3294–3298. [CrossRef]

7. Navarro-Quezada, A.; Stefanowicz, W.; Li, T.; Faina, B.; Rovezzi, M.; Lechner, R.; Devillers, T.; d'Acapito, F.; Bauer, G.; Sawicki, M.; et al. Embedded magnetic phases in (Ga,Fe)N: The key role of growth temperature. *Phys. Rev. B* **2010**, *81*, 205206. [CrossRef]

8. Navarro-Quezada, A.; Devillers, T.; Li, T.; Bonanni, A. Planar arrays of magnetic nanocrystals embedded in GaN. *Appl. Phys. Lett.* **2012**, *101*, 081911. [CrossRef]

9. Coey, J.; Smith, P. Magnetic Nitrides. *J. Magn. Magn. Mater.* **1999**, *200*, 405–424. [CrossRef]

10. Jeff, R.; Yun, M.; Ramalingam, B.; Lee, B.; Misra, V.; Triplett, G.; Gangopadhyay, S. Charge storage characteristics of ultra-small Pt nanoparticle embedded GaAs based non-volatile memory. *Appl. Phys. Lett.* **2011**, *99*, 072104. [CrossRef]

11. Li, F.; Cho, S.H.; Son, D.I.; Park, K.H.; Kim, T.W. Multilevel nonvolatile memory effect in hybrid devices containing CdSe/ZnS nanoparticle double arrays embedded in the C60 matrices. *Appl. Phys. Lett.* **2008**, *92*, 102110. [CrossRef]

12. Chang, T.C.; Jian, F.Y.; Chen, S.C.; Tsai, Y.T. Developments in nanocrystal memory. *Mater. Today* **2011**, *14*, 608–615. [CrossRef]

13. Tsunoda, M.; Takahashi, H.; Kokado, S.; Komasaki, Y.; Sakuma, A.; Takahashi, M. Anomalous Anisotropic Magnetoresistance in Pseudo-Crystal Fe_4N Films. *Appl. Phys. Express* **2010**, *3*, 113003. [CrossRef]

14. Matar, S.; Demazeau, G.; Siberchicot, B. Magnetic particles derived from iron nitride. *IEEE Trans. Magn.* **1990**, *26*, 60–62. [CrossRef]

15. Rovezzi, M.; d'Acapito, F.; Navarro-Quezada, A.; Faina, B.; Li, T.; Bonanni, A.; Filippone, F.; Bonapasta, A.; Dietl, T. Local structure of (Ga,Fe)N and (Ga,Fe)N:Si investigated by X-ray absorption fine structure spectroscopy. *Phys. Rev. B* **2009**, *79*, 195209. [CrossRef]

16. Navarro-Quezada, A.; Swacki, N.G.; Stefanowicz, W.; Li, T.; Grois, A.; Devillers, T.; Rovezzi, M.; Jakieła, R.; Faina, B.; Majewski, J.; et al. Fe-Mg interplay and the effect of deposition mode in (Ga,Fe)N doped with Mg. *Phys. Rev. B* **2011**, *84*, 155321. [CrossRef]

17. Grois, A.; Devillers, T.; Li, T.; Bonanni, A. Planar array of self-assembled $Ga_xFe_{4-x}N$ nanocrystals in GaN: Magnetic anisotropy determined via ferromagnetic resonance. *Nanotechnology* **2014**, *25*, 395704. [CrossRef]

18. Navarro-Quezada, A.; Aiglinger, M.; Gas, K.; Matzer, M.; Faina, B.; Adhikari, R.; Sawicki, M.; Bonanni, A. Magnetotransport in phase-separated (Ga,Fe)N with g-$Ga_yFe_{4-y}N$ nanocrystals. *arXiv* **2018**, arXiv:1809.08894.

19. Bianco, L.D.; Spizzo, F.; Li, T.; Adhikari, R.; Bonanni, A. Influence of Mn co-doping on the magnetic properties of planar arrays of $Ga_xFe_{4-x}N$ nanocrystals in a GaN matrix. *Phys. Rev. B* **2016**, *94*, 085205. [CrossRef]

20. Simbrunner, C.; Sitter, H.; Bonanni, A. Fourier analysis applied on in situ laser reflectometry during III-nitride metal organic chemical vapor deposition growth. *J. Appl. Phys.* **2007**, *101*, 093501. [CrossRef]

21. Patterson, A. The Scherrer Formula for X-ray Particle Size Determination. *Phys. Rev.* **1939**, *56*, 978. [CrossRef]

22. Sawicki, M.; Stefanowicz, W.; Ney, A. Sensitive SQUID magnetometry for studying nanomagnetism. *Semicond. Sci. Technol.* **2011**, *26*, 064006. [CrossRef]

23. Gas, K.; Sawicki, M. A practical solution for high-precision and high-sensitivity magnetometry in nanomagnetism and material science. *arXiv* **2018**, arXiv:1809.02346.

24. Houeben, A.; Burghaus, J.; Dronskowski, R. The Ternary Nitrides $GaFe_3N$ and $AlFe_3N$: Improved Synthesis and Magnetic Properties. *Chem. Mater.* **2009**, *21*, 4332–4338. [CrossRef]

25. Burghaus, J.; Sougrati, M.; Moechel, A.; Houben, A.; Hermann, R.P.; Dronskowski, R. Local ordering and magnetism in $Ga_{0.9}Fe_{3.1}N$. *J. Solid State Chem.* **2011**, *184*, 2315–2321. [CrossRef]

26. Kleibert, A.; Balan, A.; Yanes, R.; Derlet, P.M.; Vaz, C.A.F.; Timm, M.; Rodríguez, A.F.; Béché, A.; Verbeeck, J.; Dhaka, R.S.; et al. Direct observation of enhanced magnetism in individual size- and shape-selected 3*d* transition metal nanoparticles. *Phys. Rev. B* **2017**, *95*, 195404. [CrossRef]